Plastic deformation of Fe–Al polycrystals strengthened with Zr-containing Laves phases
I. Microstructure of undeformed materials

A. Wasilkowska [a,1], M. Bartsch [a], F. Stein [b], M. Palm [b], K. Sztwiertnia [c],
G. Sauthoff [b], U. Messerschmidt [a,*]

[a] *Max-Planck-Institut für Mikrostrukturphysik, Weinberg 2, D-06120 Halle (Saale), Germany*
[b] *Max-Planck-Institut für Eisenforschung, Max-Planck-Str. 1, D-40074 Düsseldorf, Germany*
[c] *Institute of Metallurgy and Materials Science, Polish Academy of Sciences, ul. Reymonta 25, PL-30059 Krakow, Poland*

Abstract

The microstructures of several Fe-rich Fe–Al–Zr alloys have been studied as a basis of investigating the mechanical behaviour, which is subject of Part II. The alloys with only low Zr contents show microstructures with a relatively soft matrix and a hard skeleton along the grain boundaries, the latter being residual eutectics containing the matrix phase and the $Zr(Fe,Al)_2$ Laves phase. Scanning electron microscopy, orientation imaging microscopy as well as transmission electron microscopy and diffraction are used to study the grain sizes, the orientation relationships between the grains and the phases and the crystallography of the Laves phase. With higher Zr contents above about 10 at.%, the matrix is formed by the $Zr(Fe,Al)_2$ Laves phase.
© 2004 Elsevier B.V. All rights reserved.

1. Introduction

Fe–Al based alloys are of interest as materials for structural applications due to their outstanding oxidation resistance, good mechanical strength and relatively low weight (density of 5.76–$6.32\,\mathrm{g\,cm^{-3}}$) [1]. α-Fe dissolves up to 52 at.% Al, which gives rise to various states of atomic order in the bcc lattice with concentration-dependent transformation temperatures [2]. Alloys with an Al content between 40 and 50 at.% show the B2 lattice symmetry of FeAl at temperatures up to the melting point, whereas the D0₃ structure of the alloys with about 25 at.% is stable only at lower temperatures and transforms to the B2 structure at about 550 °C. At temperatures below 550 °C, alloys with about 20–23 at.% Al are two-phase materials with the disordered α-Fe(Al) phase (A2 structure) and the D0₃ Fe₃Al phase [1]. The wide off-stoichiometric solubility range of B2 Fe–Al leads to only partial atomic order with constitutional defects.

The Al content and especially the lattice order have a pronounced influence on the room temperature mechanical properties of the iron aluminides Fe₃Al and FeAl [3,4]. Strong effects of the microstructure were observed in cast or powder metallurgically processed alloys [5]. For the development of Fe-rich aluminide base alloys, strengthening by second phases, i.e. carbides, nitrides, oxides and intermetallic phases, is attractive [5–8]. Studies on similar ternary systems show that alloying with Laves phase-forming elements has a very strong hardening effect [9,10]. In particular, NiAl with the ordered cubic B2 structure can be alloyed with Nb or Ta to produce two-phase alloys with strengthening precipitate particles and grain boundary layers containing the ternary phases $Nb(Ni,Al)_2$ or $Ta(Ni,Al)_2$. In close analogy, addition of Zr to Fe–Al alloys leads to $Zr(Fe,Al)_2$ Laves phase-strengthened iron aluminides via conventional ingot metallurgy methods [11]. The phase relations and equilibria in the Fe–Zr and Fe–Al–Zr systems

---

* Corresponding author. Tel.: +49-345-5582-927;
fax: +49-345-5511223.
E-mail address: um@mpi-halle.de (U. Messerschmidt).
[1] Present address: TU München, Lehrstuhl für Materialwissenschaft und Mechanik, Boltzmannstr. 15, D-85748 Garching, Germany

have been studied recently, and isothermal sections of the Fe–Al–Zr phase diagram have been newly established [11–13]. It is known that small additions of Zr to disordered Fe–Al alloys with low Al contents improve the oxide scale adherence and thereby the oxidation resistance at elevated temperatures [14], whereas controversial effects have been reported for the iron aluminides with higher Al contents [15,16].

A first survey of the mechanical properties of Laves phase strengthened alloys of the Fe–Al–Zr system has been given in [13]. The present work aims at a more detailed study of the mechanical behaviour of Fe–Al–Zr alloys with a strengthening Laves phase, including the strain rate sensitivity of the flow stress and the microstructure of deformed samples of selected materials of this system. First results were presented in [17]. In Part I of this paper, scanning electron microscopy (SEM), orientation imaging microscopy (OIM) and high-voltage transmission electron microscopy (HVTEM) have been employed to examine the microstructure of several materials of the Fe–Al–Zr alloy system. The mechanical properties of selected materials are described in Part II [18].

2. Experimental

2.1. Preparation of alloys

The alloys investigated in this study were prepared by vacuum induction melting using high-purity starting materials [11–13]. Their compositions are marked in Fig. 1, an isothermal section of the phase diagram [13]. Pure Fe, Al and Zr were molten under argon at 700 mbar in a ZrO_2 crucible and cast into a cold Cu mould. The shape of the ingots was cylindrical, with diameters of 10–25 mm and a maximum length of 200 mm. Specimens were sealed in quartz tubes filled with argon, annealed and subsequently quenched in NaCl brine. The annealing conditions were 500 h at 800 °C or 100 h at 1150 °C.

2.2. Characterization of the microstructure and the crystal structure

Conventional methods of surface preparation including polishing were applied for metallographic studies of the microstructure. Samples were investigated in an SEM equipped with a commercial energy-dispersive X-ray analysis system (EDX). Images were taken with a two-sector detector for back-scattered electrons with signal addition (composition mode). The volume fraction f of the phases and the surface area of phase boundaries per unit volume S were determined by superimposing a square grid onto the SEM micrographs with high magnification and counting the number P_P of intersection points of the lines of the grid that lie in the phase of interest per total number of intersection points of the grid and the number P_L of intersections of grid lines with phase boundaries per unit line length. According to standard stereological relations [19], $f = P_P$ and $S = 2P_L$. The grain size of the matrix phase was determined on SEM or orientation topography images by converting the measured grain area to the equivalent circle diameter. Orientation imaging microscopy (OIM) using the electron back-scattered diffraction technique was employed to characterize the orientation relationships between the matrix grains [20]. Two rectangles of $91 \times 127\ \mu m^2$ were scanned for this study including about 70 000 single orientations. A three-dimensional misorientation distribution function (MODF) [21] was calculated in order to recognize the tendencies in the misorientation density more precisely. Morphological parameters, e.g. the grain size, were calculated from the data with the help of the program CHANNEL (HKL Technology).

The electropolishing method of Schlesier et al. [7] was applied to prepare thin foils of sufficient quality for transmission electron microscopy. The specimens were investigated in an HVTEM with an accelerating voltage of 1 MV. For determining the crystal structure, selected area diffraction patterns were examined according to conventional rules of spot-pattern indexing using standard crystallography software.
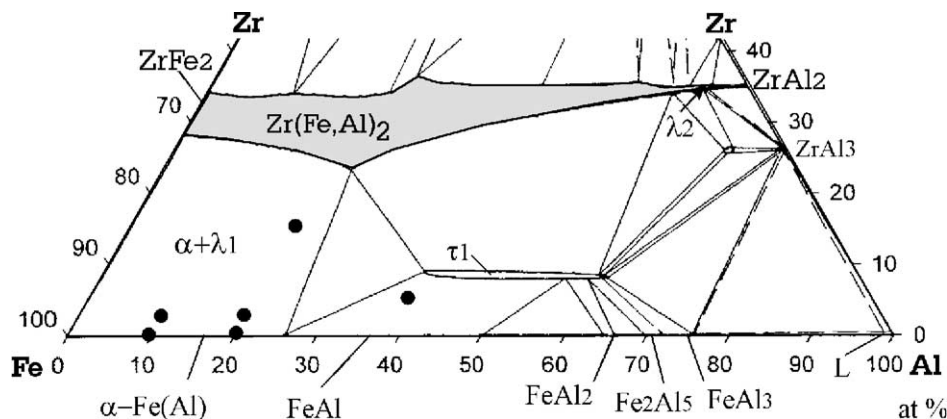

Fig. 1. Provisional isothermal Fe–ZrFe$_2$–ZrAl$_2$–Al phase diagram section at 800 °C after [11–13]. Alloys of the present study are marked by full circles (compositions are always given in at.%).

3. Experimental results

3.1. Scanning electron microscopy

Fig. 2 shows the SEM images of the microstructure of some of the alloys marked in Fig. 1, imaged in the composition mode. Zr is practically not soluble in Fe–Al according to electron microprobe analysis of selected specimens [11–13] so that second phases precipitate. The matrix grains are equiaxed. Addition of less than 10 at.% Zr causes the formation of a primary Fe–Al phase with a residual eutectic, as shown in Fig. 2(a) and (b). The bright areas correspond to the Zr-rich phase in the eutectic, the latter being distributed along the grain boundaries of the Fe–Al matrix as a hard skeleton. According to the ternary phase diagram in Fig. 1, the eutectic is composed of the $Zr(Fe,Al)_2$ Laves phase and α-Fe(Al). Addition of more than 10 at.% Zr results in the formation of a primary Laves phase again with a residual eutectic. The microstructure of Fe-22.6Al-15Zr (numbers indicate at.%) in Fig. 2(c) contains almost equal amounts of the Laves phase and the eutectic. Bright regions correspond to the Laves phase $Zr(Fe,Al)_2$. Micrographs with a high magnification were used in order to evaluate the volume fractions in the eutectic, as shown in Fig. 2(d).

Annealing leads to substantial changes of the phase morphology. The heat-treated alloy Fe-22.6Al-15Zr in Fig. 2(e) contains a bright Laves phase matrix and homogeneous dark
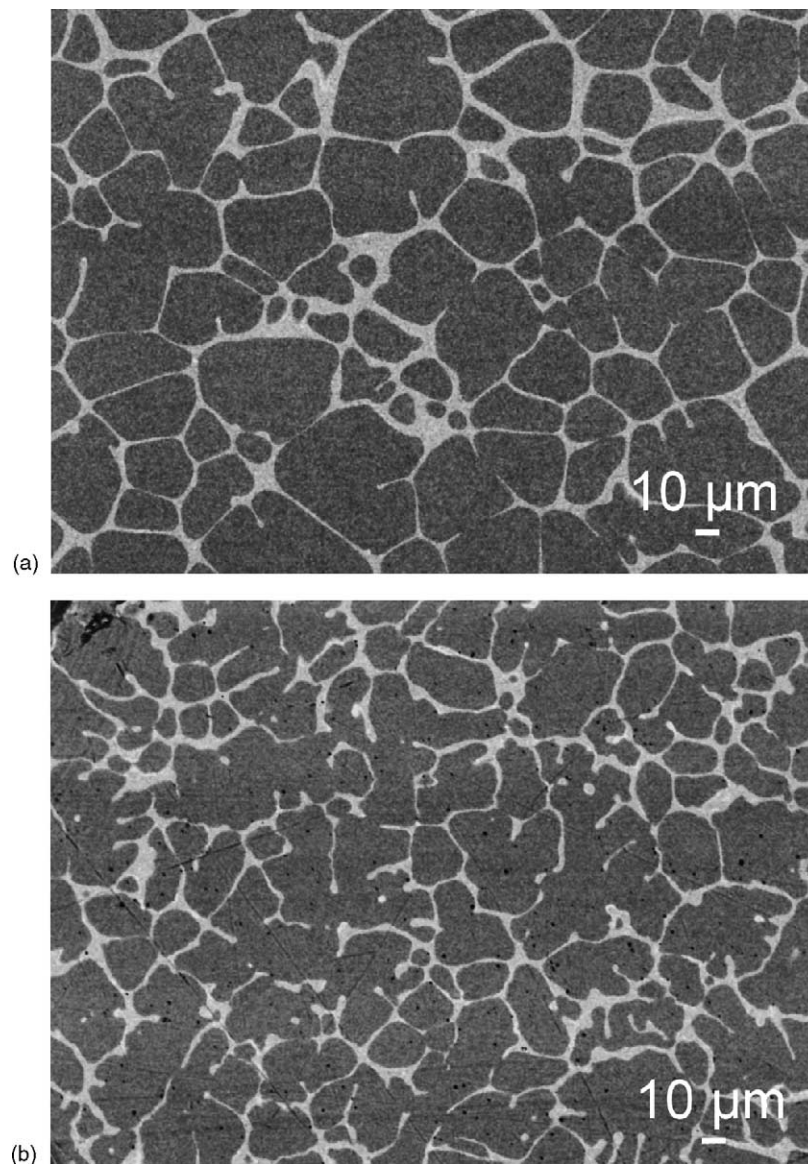

Fig. 2. Microstructure of selected alloys imaged in the SEM composition mode. (a) Fe-10Al-2.5Zr as-cast. (b) Fe-20Al-2.5Zr as-cast. (c) Fe-22.6Al-15Zr as-cast. (d) Fe-22.6Al-15Zr as-cast, structure at high magnification. (e) Fe-22.6Al-15Zr after heat treatment at 1150 °C for 100 h. (f) Fe-37.7Al-5.6Zr after heat treatment at 800 °C for 500 h (the phases corresponding to the different contrasts are described in the text; arrows in Fig. 2(e) and (f) mark a third phase).
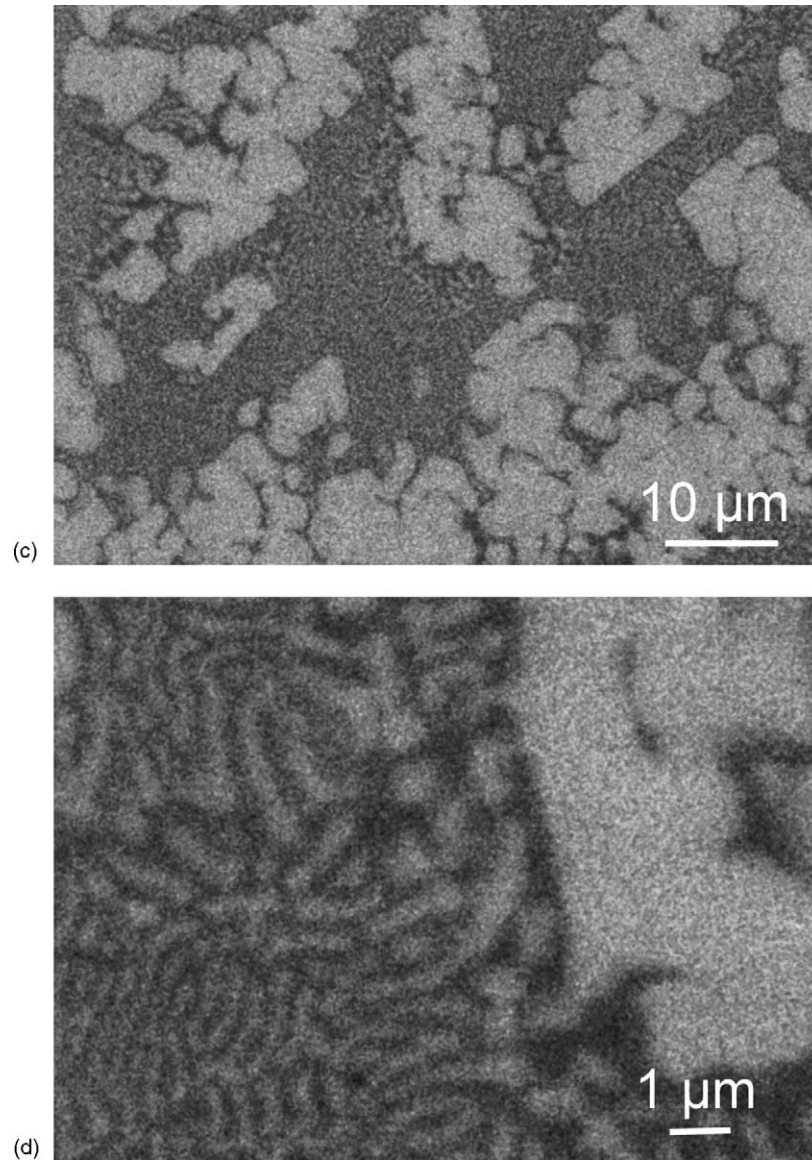
Fig. 2. (*Continued*).

regions of Fe–Al as well as a minor fraction of inclusions of a third phase (gray particles with arrows). This third phase was also detected in Fe-37.7Al-5.6Zr annealed at 800 °C (Fig. 2(f)) where it appeared as bright particles (arrows) of about 0.5 µm in size (its volume fraction does not exceed 3%).

Fig. 3 shows the volume fractions f of the alloy constituents represented as individual columns. In the eutectic, both phases are indicated separately. The numbers above the columns give the mean surface area of the constituents. For instance, in Fe-22.6Al-15Zr, the volume fraction f of single Laves phase grains amounts to 53% and their specific surface area is $S = 239\,\text{mm}^{-1}$. The remaining eutectic (47%) consists of 31 vol.% (related to the whole alloy) of the Laves phase and 16% Fe–Al with an internal surface area of $2573\,\text{mm}^{-1}$.

Both alloys with 2.5 at.% Zr, i.e. Fe-10Al-2.5Zr and Fe-20Al-2.5Zr, contain about 20 vol.% of the grain boundary eutectic. The thickness of the eutectic grain boundary layers, which are frequently interrupted, scatters in a wide range. The grain size of the alloy with 10 at.% Al is 28 µm with a broad distribution (standard deviation, 14 µm). The alloy with 20 at.% Al has a narrower distribution (standard deviation, 8 µm) with a smaller grain size of about 20 µm.

3.2. Orientation imaging microscopy

Fig. 4(a) presents an example of the orientation topography of the as-cast alloy Fe-20Al-2.5Zr. The gray scale represents the local grain orientations, showing rather a wide spectrum of orientations in the matrix. The black dots, which are more frequent at the phase boundaries and especially
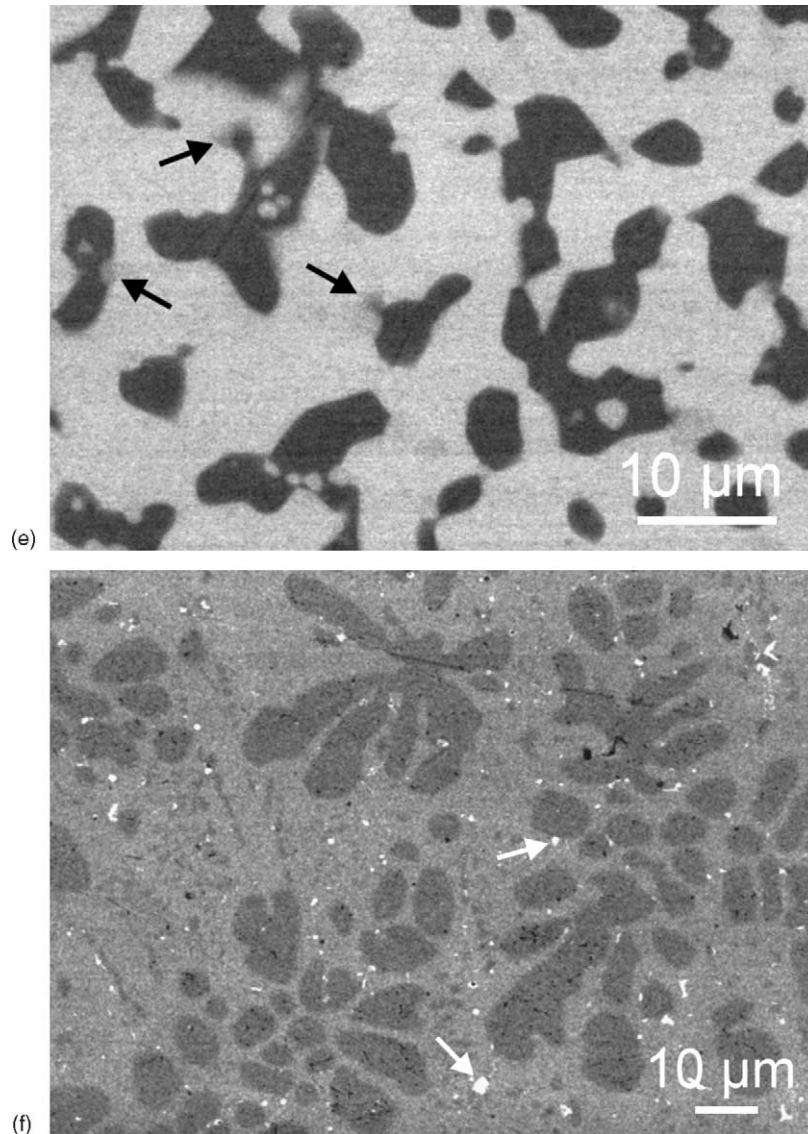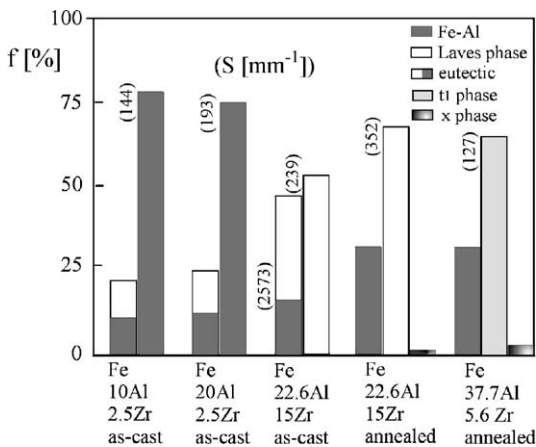
(e)

(f)

Fig. 2. (*Continued*).

Fig. 3. Volume fraction f (%) and mean surface area S (mm^{-1}) (to the left of the respective columns) of phases in the investigated alloys ($\times$phase denotes an impurity-stabilized phase, see text).

in the eutectic, correspond to spots where the orientation could not be evaluated. The orientation topographs (and also orientation distribution functions) calculated from the measured sets of single orientations of the matrix grains showed a wide spectrum of orientations randomly distributed in the sample space. A different picture was obtained when the misorientations between neighbouring grains of the matrix were determined. In Fig. 4(b), the MODF, calculated from a set of about 7500 misorientations between adjacent matrix grains, is plotted in the space of rotation axes in spherical polar coordinates (ϑ, ψ) and rotation angles ω as sections of $\omega = $ const in the region of smallest rotation angles [22]. The obtained MODF reveals some correlations characterized by maxima of ω of 20–45° around $\langle 0\,0\,1 \rangle$ and of about 45° around $\langle 2\,2\,1 \rangle$. The frequency distribution of the misorientation angles exhibits also high frequencies between 5 and 10°. The average value of the grain size from
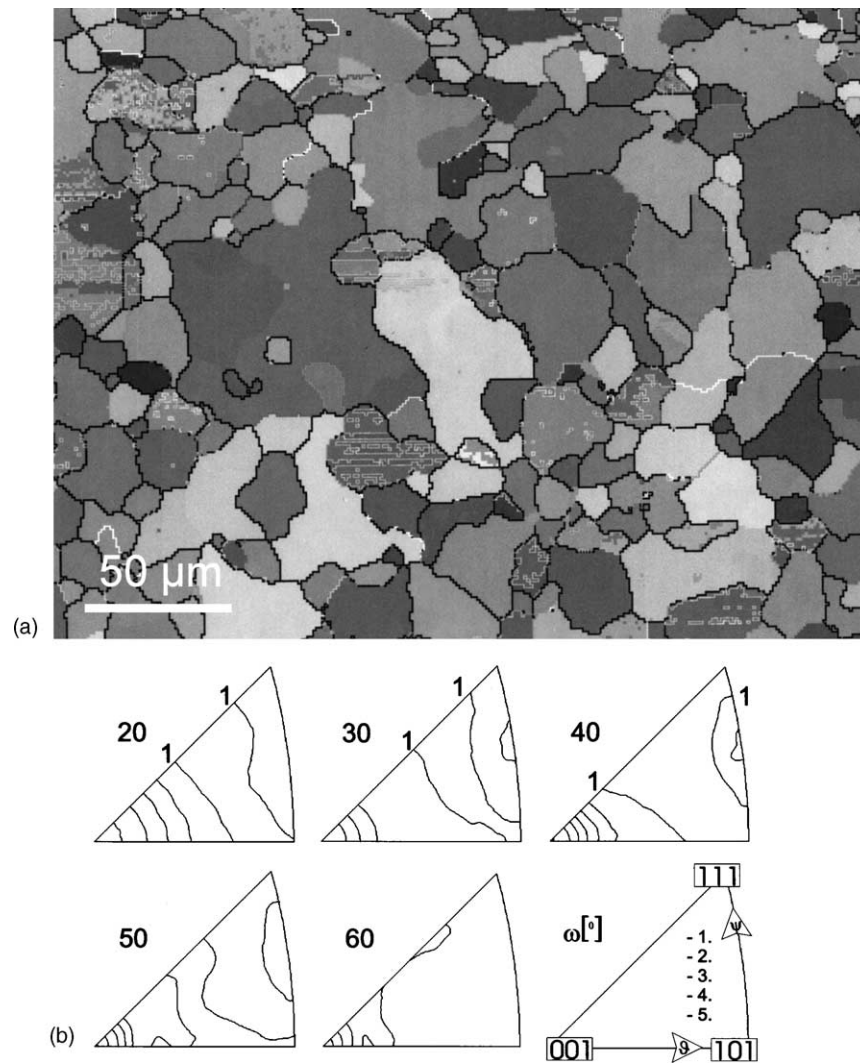
Fig. 4. OIM topography of the as-cast alloy Fe-20Al-2.5Zr. (a) orientation distribution map. (b) Misorientation distribution functions.

the OIM micrographs agrees with that of the other SEM data.

3.3. High-voltage transmission electron microscopy (HVTEM)

The microstructure and crystallography of phases was investigated by means of HVTEM. This technique makes it possible to transmit thicker specimen regions and is therefore suitable for obtaining electron diffraction patterns of two phases simultaneously. Fig. 5 shows the microstructure of Fe-10Al-2.5Zr (Fig. 5(a)) and a magnified area of the eutectic region (Fig. 5(b)). The bright contrast in the electron micrographs originates from α-Fe(Al), and the dark areas correspond to $Zr(Fe,Al)_2$. The thickness of the eutectic regions at the grain boundaries varies considerably between about 0.1 and several micrometers, and these regions are occasionally interrupted, as already noted. Diffraction patterns from the eutectic were compared with calculated ones using the experimental radii and angles of reflections. Fre-

quently, no clear correlation between the experimental and calculated patterns is found. The cubic C15 crystal structure was identified in as-cast Fe-10Al-2.5Zr (Fig. 6), and the orientation relationship is $(0\,1\,1)_{C15}||(1\,9\,5)_\alpha$, which is close to $(0\,1\,1)_{C15}||(0\,2\,1)_\alpha$, for the C15 Laves phase in contact with bcc α-Fe(Al).

In contrast to Fe-10Al-2.5Zr, the crystal structure of the Laves phase in Fe-20Al-2.5Zr was unambiguously identified as the hexagonal C14 structure. Fig. 7 shows a dark field image (Fig. 7(a)) of a eutectic region at a triple node as well as the selected area diffraction pattern of the eutectic with the Laves phase (Fig. 7(b)). The indexing of the Laves phase is given in Fig. 7(c). The observed orientation relationship is $(3\,2\,\bar{1})_{C14}||(6\,1\,\bar{3})_\alpha$. The state of atomic order in the bcc matrix is not clear. Weak super-reflections of $\{1\,0\,0\}$ type were detected in the diffraction patterns with a $(0\,0\,1)_\alpha$ zone axis only in specimens heat treated at 350 °C. These reflections indicate the B2 structure. However, other super-reflections of this structure have not been observed.
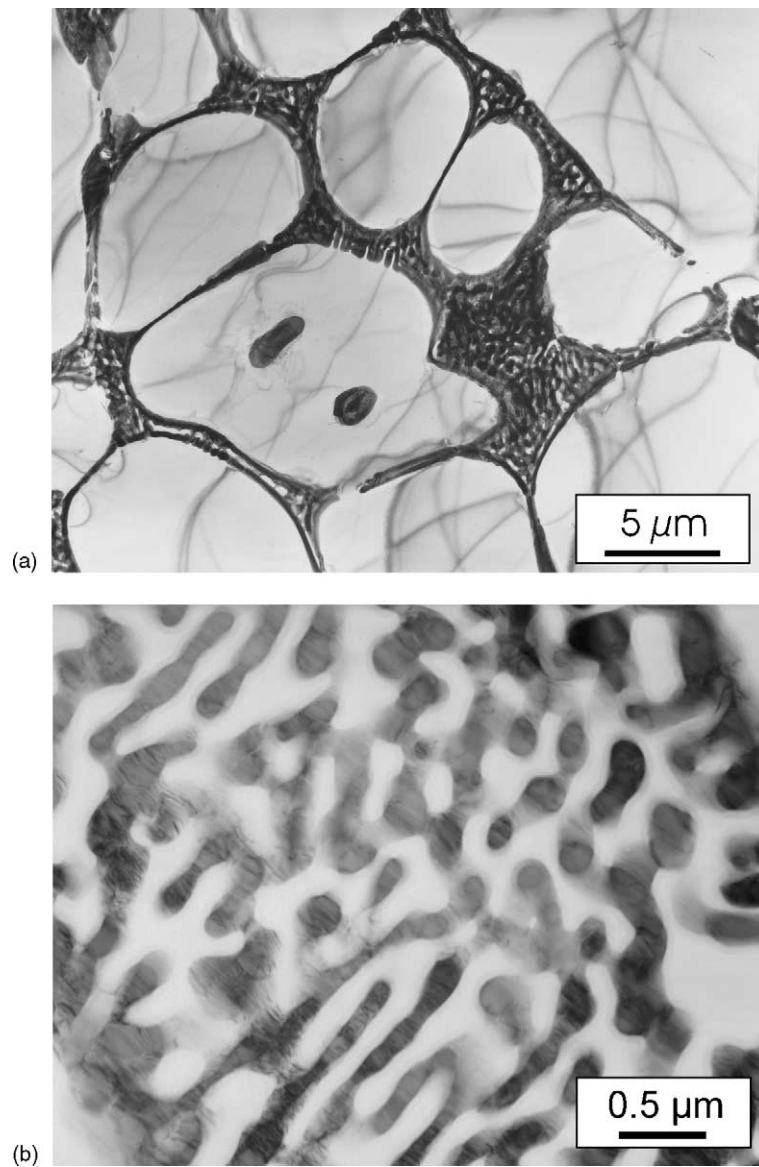
Fig. 5. HVTEM images of the microstructure of the as-cast alloy Fe-10Al-2.5Zr. (a) Overview. (b) Eutectic area at higher magnification.

The eutectic regions at the grain boundaries usually have a lamellar structure. The width of the Fe–Al lamellae was measured on micrographs where the lamellae were imaged approximately edge-on as in Fig. 5(b). The averages of about 50 Fe–Al lamellae are 0.22 and 0.16 μm for Fe-10Al-2.5Zr and Fe-20Al-2.5Zr, respectively.

Fig. 8 shows the microstructure of as-cast Fe-22.6Al-15Zr with the corresponding diffraction pattern of a single Laves phase grain. $Zr(Fe,Al)_2$ exhibits the hexagonal C14 structure.

4. Discussion

The present study shows that iron–aluminium alloys with the addition of zirconium forming the ternary Laves phase $Zr(Fe,Al)_2$ show a wide variety of microstructures. Both al-

loys with 2.5 at.% Zr, i.e. Fe-10Al-2.5Zr and Fe-20Al-2.5Zr, exhibit similar morphologies with small equiaxed grains. The $Zr(Fe,Al)_2$ Laves phase precipitates in eutectic form, distributed along the grain boundaries of the Fe–Al matrix. The volume fraction of the eutectic was about 20% in both alloys. The size of the matrix grains decreases with increasing Al content from about 28 μm for the alloy with 10 at.% Al down to about 20 μm for that with 20 at.% Al. A similar grain size dependence was reported for B2-ordered alloys containing 37–46 at.% Al [4]. At least some of the preferred misorientations between adjacent Fe–Al matrix grains in the positions of 20–45° around $\langle 0\,0\,1 \rangle$ and of about 45° around $\langle 2\,2\,1 \rangle$ correspond to coincidence site lattice (CSL) relations of $\Sigma 5 = 36.9^0 \langle 1\,0\,0 \rangle$ and $\Sigma 29b = 46.4^0 \langle 2\,2\,1 \rangle$, respectively. The orientation relationships between the matrix grains, which are separated by the residual eutectic, may result from the existence of such grain boundaries before
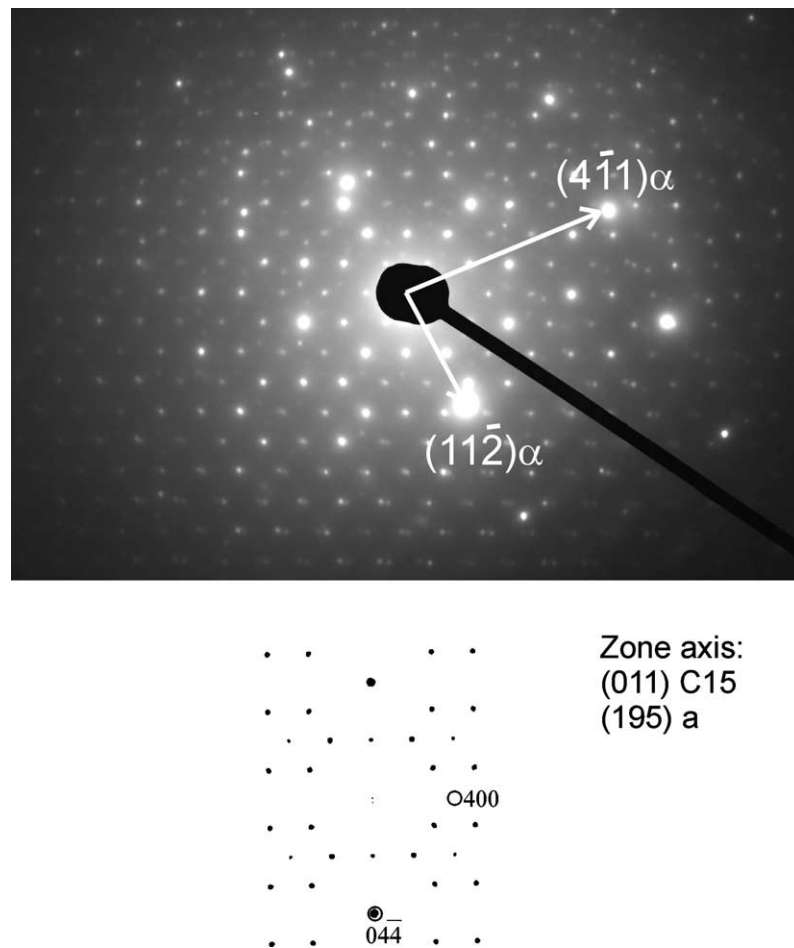
Fig. 6. Selected area diffraction pattern of eutectic region (α denotes bcc Fe(Al)).

the grain boundary skeleton was formed. Unfortunately, the orientation at the phase boundaries and especially within the eutectic cannot be evaluated by the OIM method because of its limited spatial resolution of 1 μm [20]. Studies on B2 intermetallic alloys show that low Σ boundaries (e.g. $\Sigma 1$ and $\Sigma 3$) have a higher resistance to fracture [23].

The high-index orientation relations between the Fe–Al phase and the Laves phase in the grain boundary eutectic observed by HVTEM are not a proof of the existence of coherent phase boundaries. However, the selected area diffraction aperture covers several lamellae of both phases each. The appearance of sharp diffraction spots of both phases indicates that nevertheless such relations exist.

For the mechanical properties, the ordering state of the matrix is important. In Fe-10Al-2.5Zr, the Fe–Al matrix is clearly not ordered. In Fe-20Al-2.5Zr, {1 0 0} super-reflections in the annealed specimens hint at the B2 structure, which is not consistent with the phase structure in single phase Fe–Al alloys. Possibly, the ordering state is influenced by constraints due to the presence of the hard grain boundary phase.

With increasing Zr content, the matrix changes from Fe–Al to the Laves phase. In Fe-22.6Al-15Zr, the hexagonal C14 Zr(Fe,Al)$_2$ Laves phase is present in nearly equal

amounts as matrix and eutectic precipitates. Annealing leads to substantial changes of the phase morphology resulting in a Laves phase matrix with about 23 at.% Zr and 21.5 at.% Al and isolated Fe–Al regions with 24.5 at.% Al as well as a minor fraction of a third phase. This third phase is a well-known, impurity-stabilized Fe–Zr phase with a cubic structure of the Th$_6$Mn$_{23}$ type [11–13]. The major phases in the Fe-37.7Al-5.6Zr alloy after annealing at 800 °C are the tetragonal τ_1 matrix phase Zr(Fe,Al)$_{12}$ with about 8 at.% Zr and 40.8 at.% Al and the FeAl dendrites with 30.8 at.% Al, according to Fig. 1.

An important question is the crystallographic structure of the ternary Laves phase Zr(Fe,Al)$_2$. The possible C14 and C15 structures are closely related and differ only in the particular stacking variants of long-period layer structures [24]. A number of diffraction patterns of Fe-10Al-2.5Zr could not clearly be interpreted while others could be indexed according to the C15 structure. However, the crystal structure of the Laves phase in Fe-20Al-2.5Zr with its higher Al content was clearly identified as the hexagonal C14 structure. These observations confirm the findings in [11,13].

In view of the observed microstructures, the two alloys with 2.5 at.% Zr may be attractive as structural materials
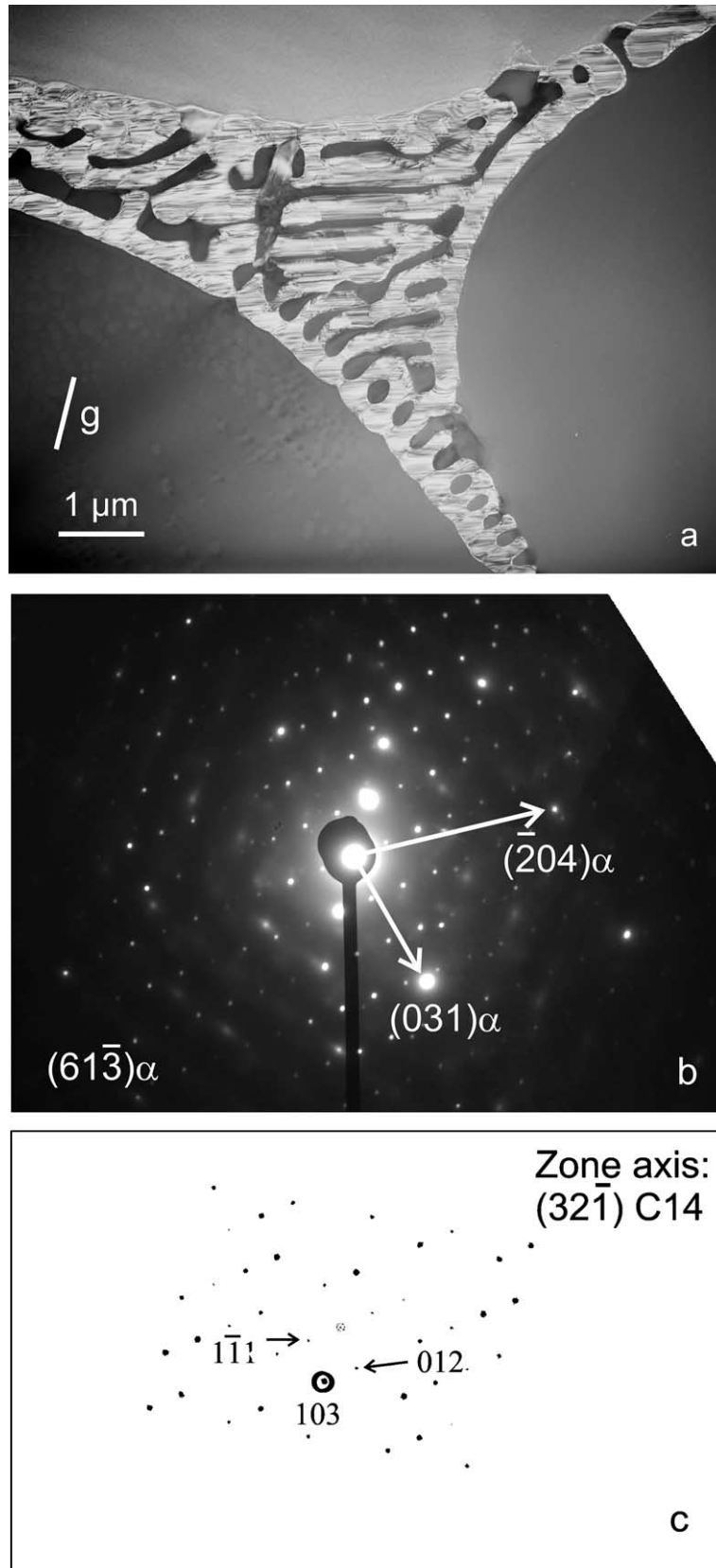
Fig. 7. Microstructure of the as-cast alloy Fe-20Al-2.5Zr. (a) Dark field image of the Laves phase using $g = (1\,0\,3)$. (b) Selected area diffraction pattern from the eutectic. (c) Computed diffraction pattern.
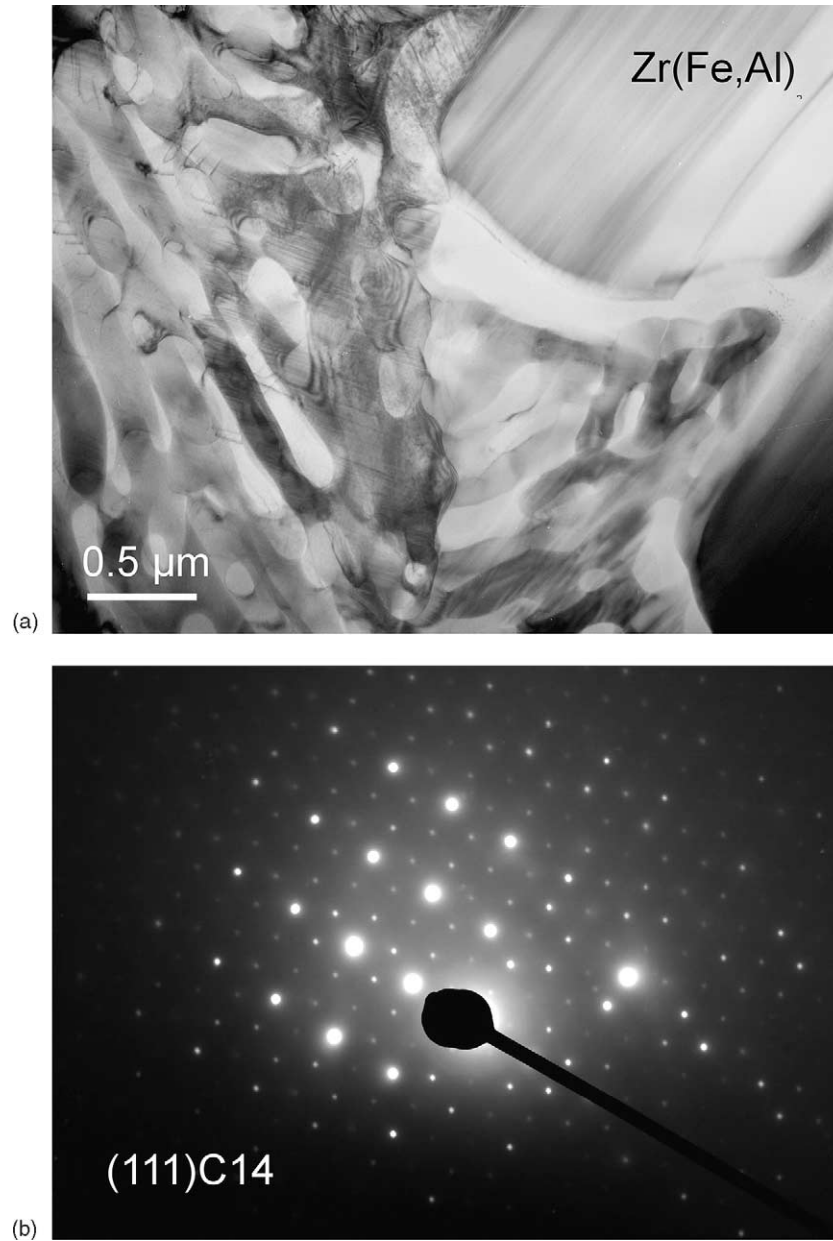
Fig. 8. Microstructure of the as-cast alloy Fe-22.6Al-15Zr. (a) Bright field image. (b) Selected area diffraction pattern from a single $Zr(Fe,Al)_2$ grain.

for intermediate to high temperatures because of their hard grain boundary skeleton with the strengthening Laves phase. Some mechanical properties of these alloys have already been reported in [13,17] according to which the high strength at room temperature is retained at higher temperatures up to almost 500 °C. This is the subject of Part II [18].

Acknowledgements

References

[1] N.S. Stoloff, Mater. Sci. Eng. A258 (1998) 1.
[2] T.B. Massalski, J.L. Murray, L.H. Bennett, H. Baker (Eds.), Binary Alloy Phase Diagrams, Materials Park OH, ASM, 1990, p. 147.
[3] G. Sauthoff, Intermetallics, VCH Verlagsgesellschaft, Weinheim, Germany, 1995, p. 84.
[4] J. Barcik, K. Stepien, T. Prandzioch, T. Mikushewski, Inzynieria Materialowa 4 (2001) 212.
[5] K. Vedula, in: J.H. Westbrook, R.L. Fleischer (Eds.), Intermetallic Compounds, Vol. 2. Chapter 9, John Willey & Sons, 1995, p. 199.

[6] D.G. Morris, Intermetallics 6 (1998) 753.

[7] C. Schlesier, J.H. Schneibel, R.P. Wahi, Z. Metalkd. 88 (1997) 810.

[8] D.G. Morris, S. Gunther, Mater. Sci. Eng. A208 (1996) 7.

[9] G. Sauthoff, Z. Metalkd. 80 (1989) 337–344.

[10] G. Sauthoff, Intermetallics 8 (2000) 1101.

[11] F. Stein, M. Palm, G. Sauthoff, In: Symposium Proceedings of Werkstoffwoche'98, Vol. VI, Wiley-VCH, Weinheim, Germany, 1998, 515.

[12] F. Stein, G. Sauthoff, M. Palm, J. Phase Equilib. 23 (6) (2002) 480–494.

[13] F. Stein, M. Palm, G. Sauthoff. Struktur und Verformungsverhalten von Fe-Al-Zr-Legierungen mit verstärkenden intermetallischen Phasen für Hochtemperaturanwendungen (Final Report DFG PA 705/3-1), 2001, p. 15.

[14] K. Wambach, J. Peters, H.J. Grabke, Mater. Sci. Eng. 88 (1987) 205–212.

[15] P.F. Tortorelli, B.A. Pint, I.G. Wright, In: Proceedings of the 11th Annual Conference on Fossil Energy Materials, ORNL/FMP-97/7, 1997, p. 235.

[16] C.H. Xu, W. Gao, H. Gong, Intermetallics 8 (7) (2000) 769–779.

[17] A. Wasilkowska, M. Bartsch, M. Palm, F. Stein, G. Sauthoff, U. Messerschmidt, In: Proceedings Conference of "20 Years Department of Physical Metallurgy and Materials Technology", March 2001, Technical University Gabrovo, Bulgaria, 2001, p. 33.

[18] A. Wasilkowska, M. Bartsch, M. Palm, F. Stein, G. Sauthoff, U. Messerschmidt, This issue.

[19] J.C. Russ, Computer-Assisted Microscopy: the Measurement and Analysis of Images, Plenum Press, New York, 1991, p. 221.

[20] D. Katrakova, C. Maas, D. Hohnerlein, F. Mücklich, Prakt. Metallogr. 35 (1998) 4.

[21] J. Pospiech, K. Sztwiertnia, F. Haessner, Textures Microstructures 6 (1986) 201.

[22] K. Sztwiertnia, J. Pospiech, F. Haessner, Textures Microstructures 12 (1990) 233.

[23] T. Watanabe, Materials Forum 11 (1988) 284.

[24] Y. Komura, Acta Crystallogr. 15 (1962) 770.